Article

A Simple and Convenient Method for Preparing Fluorine-Free Durable Superhydrophobic Coatings Suitable for Multiple Substrates

Bin Xu [1], Yinping Zhou [1], Shichang Gan [1], Qinqin Xu [1], Maohua Hou [1], Congda Lu [2],* and Zhongjin Ni [3],*

[1] College of Materials Science and Engineering, Zhejiang University of Technology, Hangzhou 310014, China
[2] College of Mechanical Engineering, Zhejiang University of Technology, Hangzhou 310014, China
[3] College of Engineering, Zhejiang Agriculture and Forestry University, Hangzhou 311300, China
* Correspondence: lcd@zjut.edu.cn (C.L.); zafu_neezj@163.com (Z.N.)

Abstract: Superhydrophobic coatings have attracted a lot of attention due to their excellent self-cleaning and anti-fouling capabilities. However, the preparation processes for several superhydrophobic coatings are intricate and expensive, which restricts their usefulness. In this work, we present a straightforward technique for creating durable superhydrophobic coatings that can be applied to a variety of substrates. The addition of C9 petroleum resin to a styrene-butadiene-styrene (SBS) solution lengthens the SBS backbone and undergoes a cross-linking reaction to form a dense spatial cross-linked structure, improving the storage stability, viscosity, and aging resistance of the SBS. The combined solution functions as a more stable and effective adhesive. Using a two-step spraying technique, the hydrophobic silica (SiO_2) nanoparticles solution was applied to the surface to create durable nano-superhydrophobic coatings. Additionally, the coatings have excellent mechanical, chemical, and self-cleaning stability. Furthermore, the coatings have wide application prospects in the fields of water–oil separation and corrosion prevention.

Keywords: superhydrophobic coatings; SiO_2; SBS; C9 petroleum resin; spraying

1. Introduction

In recent years, scientists have increasingly researched biological surfaces, including lotus leaves [1], waterfly legs [2], cicada wings [3], and other surfaces with high dust-proofing and self-cleaning functions. A large number of studies on superhydrophobic surfaces using biological surfaces as templates have revealed that a rough structure and low surface energy are necessary conditions for superhydrophobic surfaces [4–6]. The contact angle (CA) of the superhydrophobic surface is greater than 150°, and the sliding angle (SA) is less than 10°. Superhydrophobic surfaces have been widely used in self-cleaning [7], anti-icing [8], anti-corrosion [9,10], drag reduction [11], oil–water separation [12,13], and other fields. However, superhydrophobic surfaces have poor stability, and the surface is destroyed easily in special environments, such as mechanical friction or chemical corrosion. Additionally, most superhydrophobic materials have limitations such as high costs, complex fabrication processes, and a single substrate. As a result, strong superhydrophobic coatings that are low-cost, easy to apply, and can be employed on a variety of substrates are required.

At present, superhydrophobic coatings are made using a variety of techniques, including the sol–gel approach [14,15], template method [16,17], plasma etching method [18–20], chemical vapor deposition [21,22], self-assembly [23], rapid breakdown anodization [24], chemical etching [25], and others. However, the substrate is severely constrained by these procedures, because these methods of making superhydrophobic coatings are complicated and expensive. In contrast, the wet chemical processes of dipping and spraying are of particular interest, and spraying in particular is desirable. Because the spraying method is more convenient for large-scale manufacturing and less dependent on equipment, there is

no requirement for the size and shape of the substrate [26,27]. Some researchers prepared superhydrophobic coatings by mixing nanoparticles directly with adhesives with low surface energy [28–32]. The addition of nanoparticles provides a rough structure, which is an important factor in the superhydrophobic coating [33]. In early studies, silica and titanium dioxide as nanoparticles, and epoxy resin, SBS, and polydimethylsiloxane (PDMS) as common low surface energy adhesives have been widely studied in the preparation of superhydrophobic coatings. However, large amounts of nanoparticles are added, which makes the durability of the coating poor. Some other scholars have explored a strategy similar to "spraying adhesive + functional coating" to enhance the adhesion between coating and substrate, and to improve the mechanical wear resistance and durability of the surface [34,35]. First, a layer of primer resin coating is sprayed to improve the durability and stability of the coating, and then a layer of nanoparticles with low surface energy is sprayed on the surface to construct a superhydrophobic surface with roughness.

Recently, SBS was widely utilized in coatings [36], adhesives [37], inks [29,38], and other materials because of its high tensile strength, superior chemical resistance, outstanding low-temperature characteristics, and low cost. SBS has been widely employed to create superhydrophobic coatings in recent years [29–32]. Some scholars prepared superhydrophobic coatings by mixing SBS and nanoparticles with low surface energy directly in an organic solvent. Since SBS is non-polar and has a weak van der Waals force and permeability, the bonding effect is not immediately apparent. It can have a stronger bonding effect if petroleum resin is used with it [39,40]. The storage stability, viscosity, and anti-aging of SBS have been reported to be improved by adding petroleum resin to the SBS solution, which lengthens and cross-links the SBS skeleton to produce a dense spatial cross-linked structure [36,40,41].

Based on previous work, we prepared robust superhydrophobic coatings by mixing C9 petroleum into SBS solution, spraying the resulting mixture as a binder layer on a glass substrate while it was still outside, and then covering the surface with a hydrophobic SiO_2 nanoparticle solution. The mass ratio of SBS to C9 petroleum resin was 1:2, and the hydrophobic SiO_2 nanoparticles content was 5 wt.% to produce the SBS, C9 petroleum resin and hydrophobic SiO_2 nanoparticles (SBS/C9-SiO_2) coatings with the optimum performance. The CA was 155.6° ± 1° and the SA was 4.1° ± 0.5° when SBS/C9-SiO_2 coatings were put on the glass surface. Spraying the coatings onto a variety of different substrates, such as paper, press cloth, metal, and so on, also rendered it superhydrophobic. The SBS/C9-SiO_2 coatings have corrosion resistance and can be used in oil–water separation equipment. The method did not need expensive or sophisticated equipment and had a wide range of possible applications.

2. Materials and Methods

2.1. Materials

Linear SBS (YH-792) was purchased from Dongguan Jishun Rubber & Plastic Technology Co., Ltd. (Dongguan, China). C9 petroleum resin from Shenzhen Jitian Chemical Co., Ltd. (Shenzhen, China). SiO_2 nanoparticles (SK-200s, 20 nm) was supplied by NANO Technology Co., Ltd (Shaoxing, China). Ethyl acetate was obtained from Ron's reagent, acetone and ethanol were purchased from Sinopharm, and the glass slides were the Sailboat brand. The filter cloth and paper were purchased from Shaoxing Aobang Technology Co., Ltd. (Shaoxing, China). The aluminum sheet was from Shenzhen Quanfu Metal Co., Ltd. (Shenzhen, China). All chemicals were used as received.

2.2. Preparation of the Coatings

The glass slides were sonicated with ethanol and acetone for 10 min to remove surface impurities and oil stains, rinsed with deionized water, and then put into a drying oven at 80 °C for 30 min. SBS and C9 petroleum resin were dissolved in ethyl acetate and stirred at room temperature for 12 h to obtain 9 wt.% SBS and C9 petroleum resin (SBS/C9) solution, and SiO_2 nanoparticles were then dissolved in ethyl acetate and sonicated for 15 min to

produce 5 wt.% of SiO_2 hydrophobic dispersion. As shown in Figure 1, the SBS/C9 solution was first sprayed on the substrate with the high-pressure (0.2 Mpa) spray gun, kept at room temperature for 1–2 min to wait for the surface to dry, and then a layer of SiO_2 hydrophobic dispersion was sprayed with a high-pressure (0.2 Mpa) gun and left to dry at room temperature for 5 min to obtain solid SBS/C9-SiO_2 coatings. The SBS/C9-SiO_2 coatings could also be prepared by spraying the compound solution on the aluminum sheets, filter cloth, and paper in the same way.
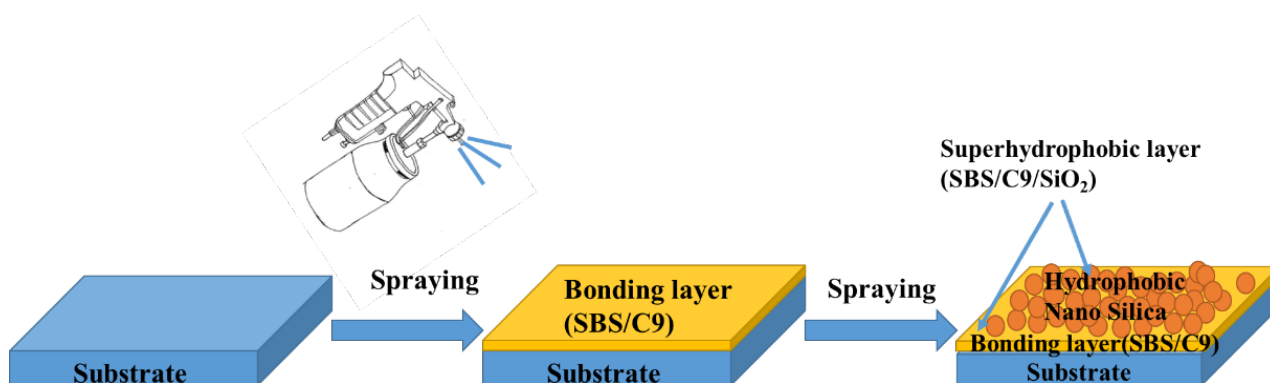
Figure 1. Schematic diagram of the preparation of SBS/C9-SiO_2 coatings on the substrate.

2.3. Characterization

The surface micromorphology of the coatings was analyzed by a ΣIGMA 300 field emission scanning electron microscope from Zeiss, Jena, Germany. Before testing, a thin layer of gold was sprayed on the sample surface to increase its electrical conductivity. The functional groups of SBS and C9 petroleum resins were analyzed using the KBr liquid film method. Spectra were recorded on films obtained from solutions after solvent evaporation, with a Fourier transform infrared spectrometer (Nexus, Thermo, Waltham, MA, USA) in the range of 400~4000 cm^{-1}. The CA and SA of SBS/C9-SiO_2 coatings were investigated using a fully automated contact angle meter OCA30 at 8 μL per drop. For each sample, three places were chosen to measure the CA and SA, and the final average value was used to determine the CA and SA of the sample. An electrochemical workstation (CHI 660, Shanghai) was used to test the corrosion resistance of SBS/C9-SiO_2 coatings. In a 3.5 wt.% NaCl electrolyte solution, saturated potassium chloride was used as the reference electrode, a platinum electrode (Pt) served as the counter electrode, and an exposed 3.14 cm^2 sample served as the working electrode. The kinetic potential polarization curves of substrates coated with SBS/C9-SiO_2 on 316 stainless steel and Al were measured. The mechanical stability of the coatings was tested by friction with sandpaper. The glass coated with SBS/C9-SiO_2 was immersed in three different solutions of sodium chloride solution (3 wt.%), hydrochloric acid solution (pH = 1), and ammonia solution (pH = 13) for 24 h, respectively, in order to test the chemical stability of the coatings.

3. Results

3.1. Tape Peel Cycle Test

The content of SBS in the adhesive layer remained constant at 3 wt.%, whereas the content of C9 petroleum resin grew gradually from 0 to 8 wt.%, and SiO_2 nanoparticles were dissolved in ethyl acetate to produce 5 wt.% of SiO_2 hydrophobic dispersion. When the C9 petroleum resin content is 0, the coatings are recorded as SBS-SiO_2. The SBS/C9-SiO_2 coatings with various C9 petroleum resin concentrations were applied to the glass surface by the two-step spraying method. We counted the instances in which the SBS/C9-SiO_2 coatings could be peeled off the tape after it had dried, or instances in which the coatings either lost their superhydrophobic properties or their CA dropped below 150°. The tape may be peeled off more times thanks to C9 petroleum resin, as shown in Figure 2. This is because C9 petroleum resin increased the number of times the tape peel cycles the

SBS/C9-SiO$_2$ coatings. The addition of C9 petroleum resin makes the skeleton of SBS longer, and the cross-linking reaction occurs to form a dense spatial cross-linking structure, which improves the storage stability, viscosity, and anti-aging properties of SBS/C9 coatings [42]. When the addition of C9 petroleum resin was 6 wt.%, the coatings had the best mechanical properties and could be peeled by the tape up to 65 times.
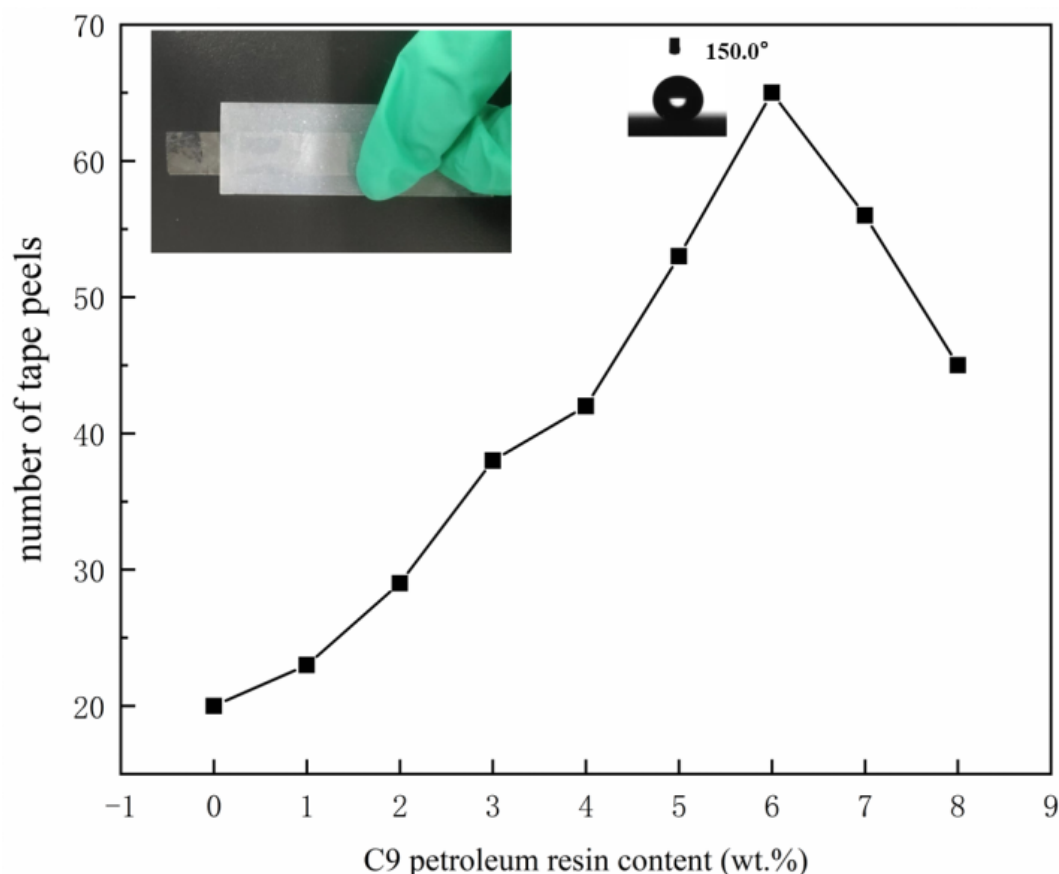
Figure 2. Relationship between the content of C9 petroleum resin and the number of stripping cycles of the SBS/C9-SiO$_2$ coating.

### 3.2. Superhydrophobic Coatings Applied to a Variety of Substrates

Dataphysics's OCA30 automatic contact angle measuring instrument was used to measure the CA. Due to the low surface tension of the SBS/C9-SiO$_2$ coatings and the 4 μL water droplet having light gravity, it was difficult to adhere to the surface of the coating. As shown in Figure 3a, a 4 μL drop of water was squeezed out of the dropper of the contact angle meter and slowly lowered to touch and squeeze to the surface of SBS/C9-SiO$_2$ coatings, and then lifted the dropper to separate the drop from the surface. Although the water droplets were squeezed and deformed on the surface of the coating, there was no liquid residue on the surface of the coatings after separation, and the droplets recovered to their original state. The above results demonstrated that the coatings had low adhesion to water. As shown in Figure 3b, we employed 8 μL of water droplets and let them fall on the surface of the SBS/C9-SiO$_2$ coatings by gravity, then tested the CA of the coatings on aluminum sheets, filter cloth, paper, and glass surfaces, and found that all their CAs were larger than 150°. The SA of the coatings on the substrates was tested using 10 μL of water droplets, and the SAs were all less than 10°, indicating that they all obtained sensational superhydrophobicity.
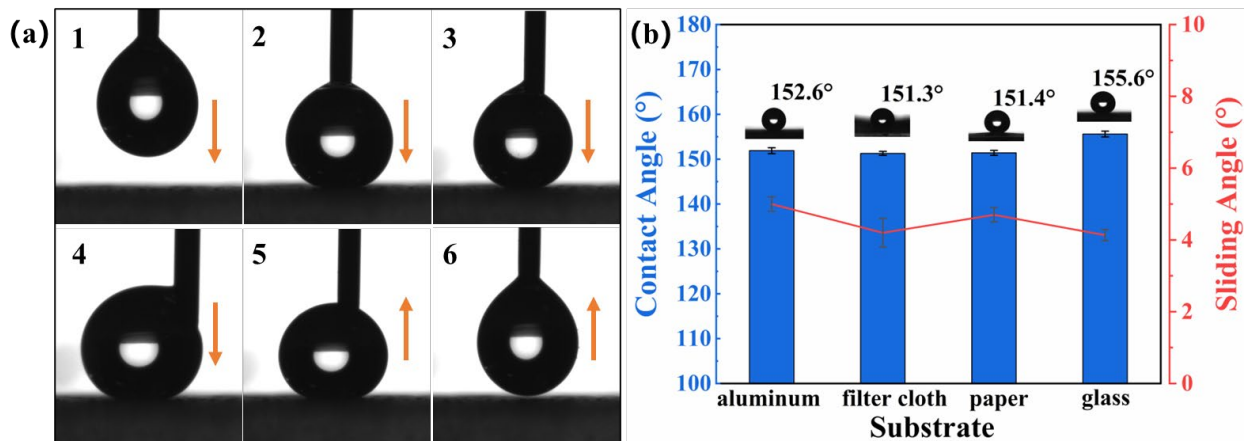
Figure 3. (**a**) Picture of water droplets squeezed and re-lifted on the SBS/C9-SiO$_2$ coatings' surface. (**b**) CA and SA of SBS/C9-SiO$_2$ coatings on different substrates.

3.3. Surface Wettability and Morphology

Figure 4 shows the microscopic morphology and WCA images of the clean glass, SBS/C9 coatings, and SBS/C9-SiO$_2$ coatings' surface. As demonstrated in Figure 4a, the surface of the untreated clean glass was highly smooth, with a CA of 44.3° ± 1°. As illustrated in Figure 4b, the surface with the SBS/C9 coatings displayed some irregular micro-scale protrusions, and the WCA was 81.7° ± 1° while still maintaining a hydrophilic state. The surface structure following the SBS/C9-SiO$_2$ coatings is shown in Figure 4c–e, indicating a multi-scale rough structure, and the surface had a lotus-like surface papillary structure [43] that was formed by the aggregation of the nanoparticles' uneven aggregates. Figure 4e indicates a surface with many pores of different sizes, which might be explained by the "respiration diagram" [44], which was caused by the high relative humidity of the air when the SBS/C9-SiO$_2$ coatings were dry in the air. At this time, the CA of the SBS/C9-SiO$_2$ coatings was 155.6° ± 1°, showing a superhydrophobic state, which was mainly determined by the micro-scale pores, SiO$_2$ nanoparticle aggregation, and the multi-scale roughness of SiO$_2$ nanoparticles.
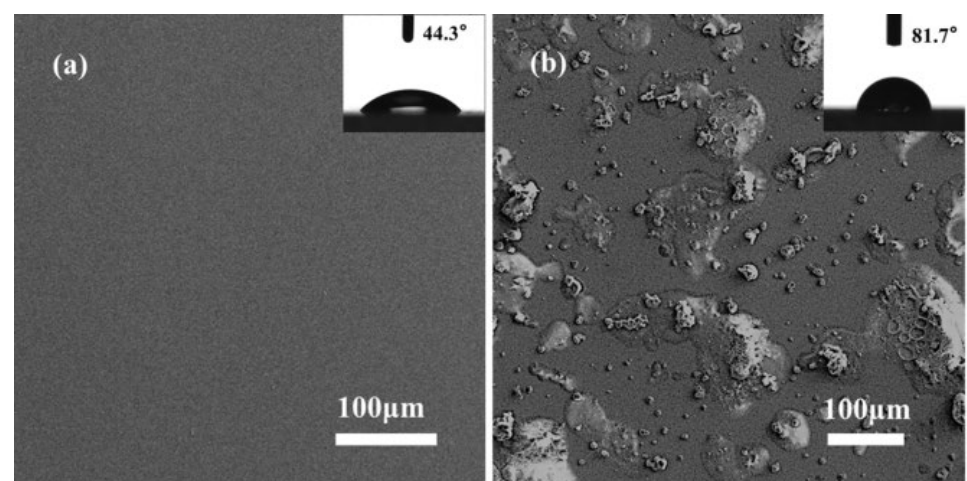
Figure 4. *Cont.*
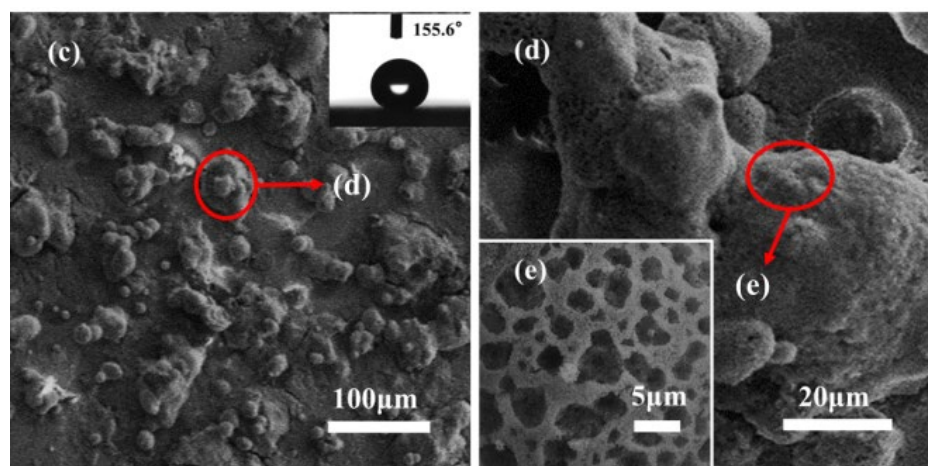
Figure 4. Surface of (**a**) clean glass, (**b**) SBS/C9 coatings, and (**c–e**) SBS/C9-SiO$_2$ coatings under SEM pictures and CA pictures.

3.4. Surface Composition Analysis

As shown in Figure 5, in the functional group region (4000~1300 cm^{-1}), the absorption peaks at 3000~2800 cm^{-1} in the spectra of the SBS/C9 mixture represent the bending vibration of symmetric methylene on the SBS skeleton and the stretching vibration of a C-H bond saturated with C9 petroleum resin. The absorption peak at 1738 cm^{-1} is characteristic of the carbonyl group, due to the presence of ethyl acetate. The peak at 1600 cm^{-1} is the respiratory vibration peak of the benzene skeleton. The peaks at 1490 cm^{-1} and 1448 cm^{-1} are the flexion vibrations of saturated C-H bonds of the SBS and C9 petroleum resins. In the fingerprint region (1300~400 cm^{-1}), the peak at 972 cm^{-1} may be offset by the peak of the SBS and C9 petroleum resins at around 1070 cm^{-1}, which may be due to the existence of van der Waals forces between them. The peak at 969 cm^{-1} is the absorption peak of the butadiene trans vibration of the SBS. The peak at 910 cm^{-1} is the in-plane vibration of the SBS trans double bond hydrocarbon. The peaks at 749 cm^{-1} and 700 cm^{-1} are the out-of-plane bending vibrations of the benzene C-H bond of the SBS and C9 petroleum resins. There was no obvious change in the mixture spectra, which indicated that the SBS and C9 petroleum resins were physically doped [45].
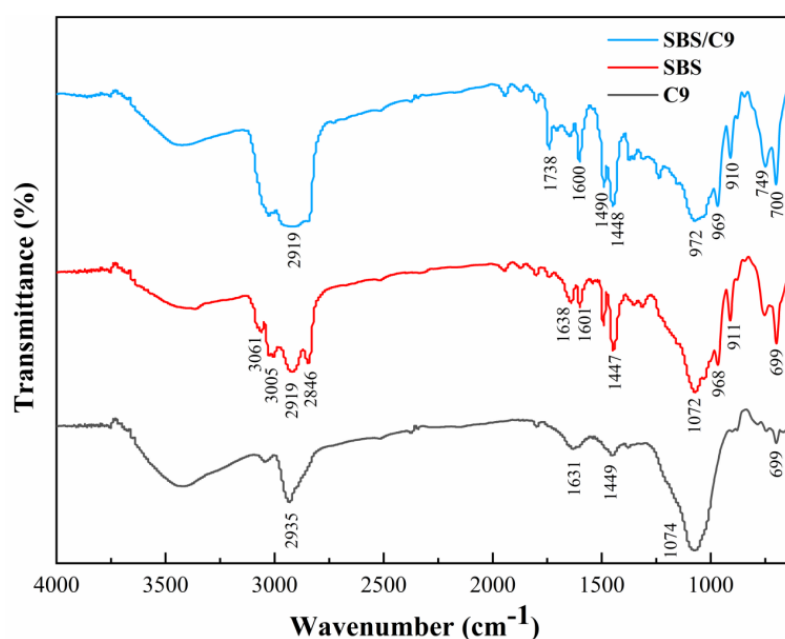

Figure 5. FTIR spectra of SBS, C9 petroleum resin, and SBS/C9.

3.5. Mechanical Performance Test

Figure 6a shows a schematic diagram of the sandpaper abrasion test. The sample was applied uniformly onto 800 mesh sandpaper after a 100 g weight was placed on the glass. The distance between each abrasion movement was 20 cm, and the CA of the sample was measured after 10 abrasions, as shown in Figure 6b. As shown in Figure 6c, the SBS-SiO$_2$ coatings were badly worn after 50 rubbings, with a CA of $142.8° \pm 3°$. The severely worn areas exposed the glass substrate, and water droplets did not roll off the surface easily, even though the water contact angle hysteresis was severe. As shown in Figure 7d, there was no significant change in the wettability of the SBS/C9-SiO$_2$ coatings after 65 abrasions, with a CA of $149.8° \pm 1°$. The droplets rolled off the surface easily, despite some of the SiO$_2$ nanoparticles having worn off. The reason for this is that the SBS/C9 binder is coated with a layer of nanoparticles during the curing process, which enhances the bond strength between the nanoparticles and the substrate. In addition, the SBS/C9 liquid binder forms micron-sized protrusions when bent, which protect the nanoparticles on the sidewalls and between the protrusions during the wear process, thus improving the mechanical durability of the surface.
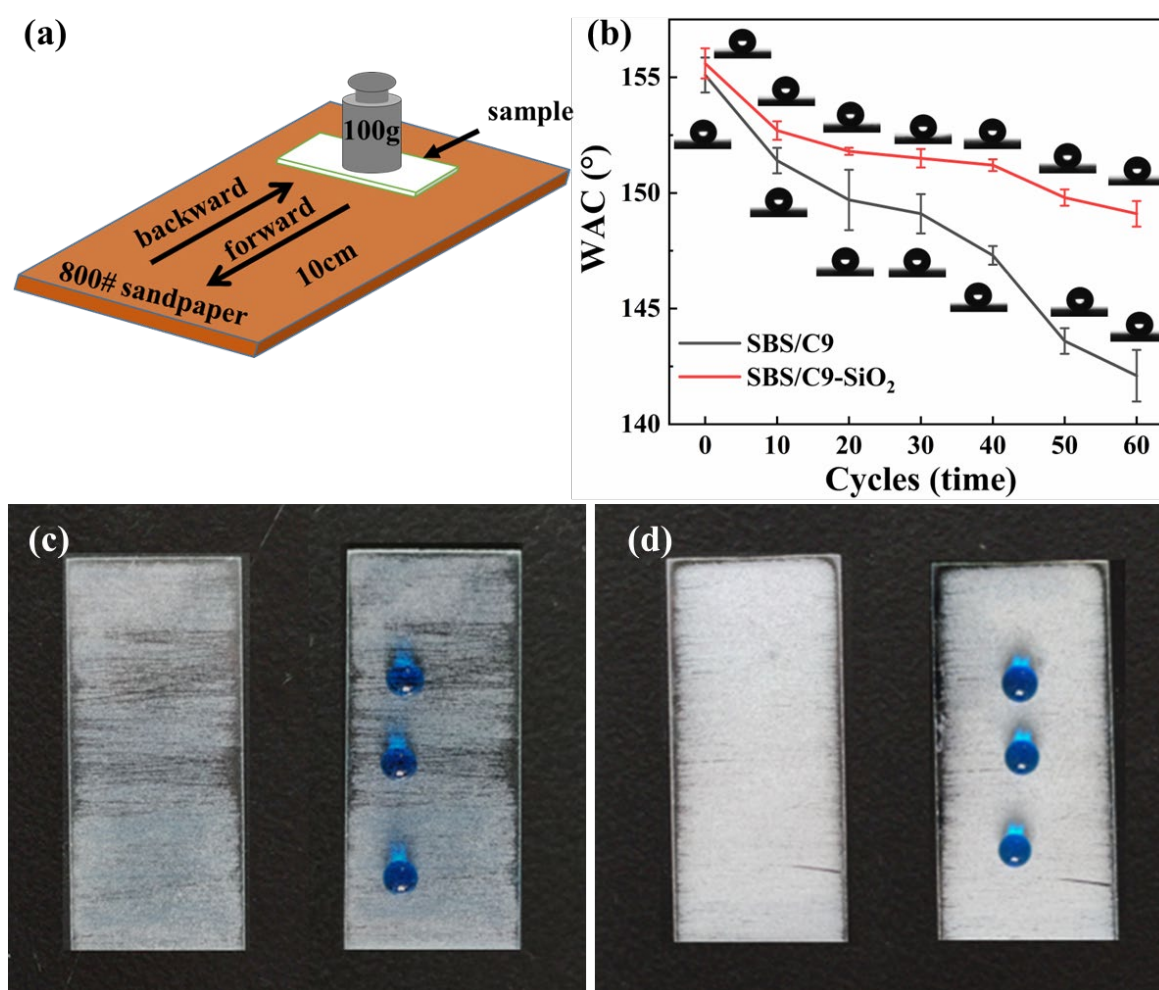
Figure 6. (**a**) Schematic diagram of abrasion resistance test of sandpaper; (**b**) relationship between abrasion times and the CA of the SBS-SiO$_2$ coatings and SBS/C9-SiO$_2$ coatings; image of the (**c**) SBS-SiO$_2$ coatings and (**d**) SBS/C9-SiO$_2$ coatings after 60 rubbings.
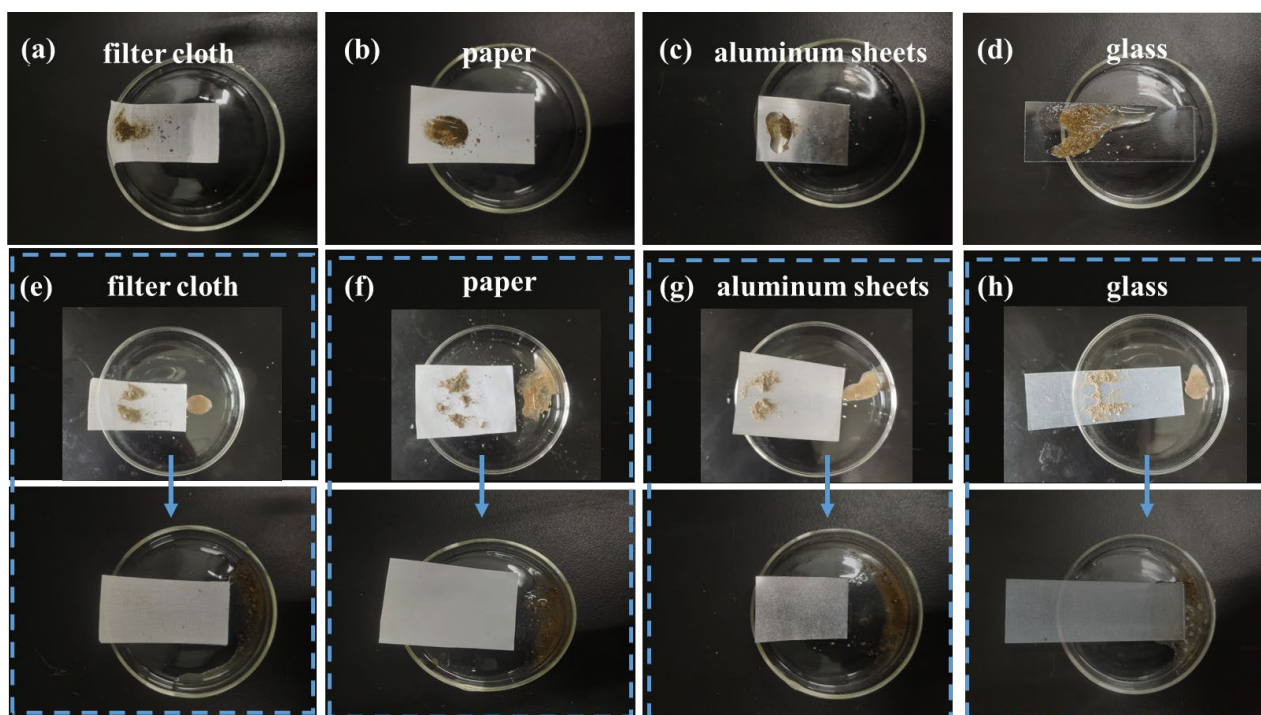
**Figure 7.** The self-cleaning experiment of SBS/C9-SiO$_2$ coatings.

3.6. A Self-Cleaning Performance of the Superhydrophobic Coatings

As shown in Figure 7, the slide coated with superhydrophobic coatings was placed at an angle. To facilitate observation, we placed the soil on the surface of the glass slide, and then water drops were dropped from the top end of the samples with a dropper. As the water drops rolled down, the soil on the surface rolled with them, and the surface became very clean after a while. On the one hand, the low adhesion of the superhydrophobic coatings to water droplets made it easy for water droplets to roll the across surface and difficult for them to stay on there. On the other hand, since the affinity between the soil and water droplets was larger than the affinity between soil and the surface of the superhydrophobic coatings, the soil also rolls off the surface when water droplets do. This demonstrates that the superhydrophobic coatings developed in this study have strong self-cleaning properties and may be employed in real-world applications.

3.7. Chemical Stability Test of Superhydrophobic Coatings

As illustrated in Figure 8a, the sprayed glass with the SBS/C9-SiO$_2$ coatings was immersed in three different solutions of sodium chloride solution (3 wt.%), hydrochloric acid solution (pH = 1), and ammonia solution (pH = 13) for 24 h. Subsequently, we discovered that the surface of the coatings was not damaged, that it still had a satisfactory superhydrophobic effect, and that the CA was more than 150°, as shown in Figure 8b. In Figure 8a, the SBS/C9-SiO$_2$ coatings of the sample were bright silver in solution because the micro-nano structured coatings were hydrophobic and would not be in direct contact with the solution. A large amount of air was stored between the coatings and the solution, forming an air barrier that effectively prevents the irritating solution from directly touching the coatings, thus protecting the coatings from corrosion. This indicates that the coatings are resistant to corrosion and have promise for real-world applications in marine environments.
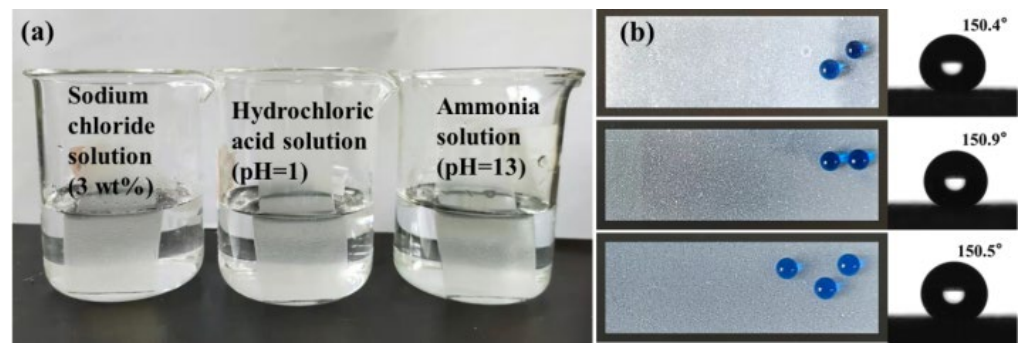
Figure 8. (**a**) The SBS/C9-SiO$_2$ coatings were soaked in sodium chloride solution (3 wt.%), hydrochloric acid solution (pH = 1), and ammonia solution (pH = 13); (**b**) glass surface with SBS/C9-SiO$_2$ coatings and CA pictures after soaking for 24 h.

3.8. Anti-Corrosion Performance of the Superhydrophobic Coatings

Corrosion resistance is frequently studied using a potentiodynamic polarization curve. The corrosion voltage corresponds to the tangent of the cathodic and anodic polarization curves, and the corrosion current density corresponds to the corrosion current density. The more negative the corrosion voltage, the greater the corrosion current, and the more likely the corrosion will occur [46]. Figure 9a,b display the potentiodynamic polarization curves of aluminum and 316 stainless steel with the SBS/C9-SiO$_2$ coatings' surfaces in 3.5 wt.% NaCl aqueous solution, respectively. After superhydrophobic treatment, the corrosion voltage of 316 stainless steel rose from -1.023 V to -0.296 V, while the corrosion current density decreased from 3.844×10^{-6} A/cm^2 to 3.272×10^{-7} A/cm^2. The corrosion voltage of Al increased from -1.334 V to -1.057 V, while the corrosion current density declined from 1.211×10^{-6} A/cm^2 to 4.314×10^{-7} A/cm^2. The results of the potentiodynamic polarization tests reveal that the corrosion current density (Icorr) of all coated samples reduced sharply compared to the bare substrates. Meanwhile, the corrosion potential (Ecorr) of all coated samples moved in a more positive direction as compared to that of the substrate, which indicates that the corrosion trend has dramatically improved and the coating effectively provides a protective way for the substrate. The air layer that forms between the SBS/C9-SiO$_2$ coating's superhydrophobicity and the NaCl solution and the resin binder causes it to generate a two-stage protective layer on the surface of multi-scale structures. Among them, the air layer effectively shields the substrate's surface from corrosion products. The air layer and resin binder form a double layer of protection and improve the substrate's ability to resist corrosion, particularly in the case of metal materials.
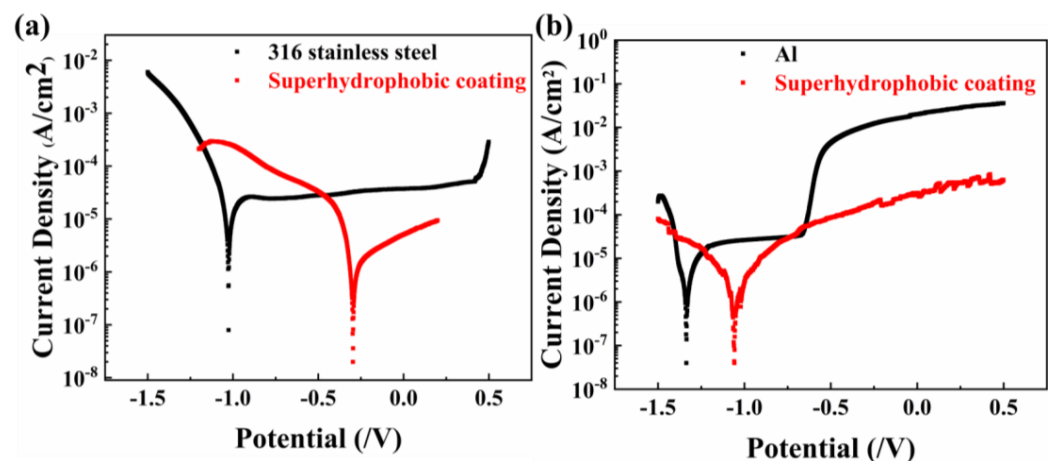
Figure 9. The potentiodynamic polarization curve of (**a**) 316 stainless steel substrate and with SBS/C9-SiO$_2$ coatings; and (**b**) Al substrate and with SBS/C9-SiO$_2$ coatings.

3.9. Oil–Water Separation of Superhydrophobic Coatings

The feasibility of the SBS/C9-SiO$_2$ coatings for oil and water separation was studied in this experiment. Because the SBS/C9-SiO$_2$ coatings are superhydrophobic and superoilphilic, the super hydrophobic filter clothes cannot be penetrated by water, yet oil with low surface energy may readily pass through. As a result, coated filter clothes are seen to be a promising material in the field of water–oil separation. The oil phase was n-hexane, and the aqueous phase was deionized water and stained with methylene blue for observation. Because n-hexane is significantly less thick than water, it floats to the surface when mixed with it. The filter cloth with the SBS/C9-SiO$_2$ coatings was put between the top and lower glass tubes. The separation of a mixture of hexane and water is depicted in Figure 10. The SBS/C9-SiO$_2$ coatings on the filter cloth allowed n-hexane to pass through and collect in a beaker below, but water stayed in the glass tube in front of the filter cloth. The result reveals that the filter cloth with the SBS/C9-SiO$_2$ coatings can separate oil and water combinations.

Figure 10. (**a**–**c**) Oil–water separation experiment of the SBS/C9-SiO$_2$ coatings.

4. Conclusions

By adding C9 petroleum resin to SBS as a binder and applying SiO$_2$ to its surface, it was possible to create a stable superhydrophobic coating with an AC of over 150° and an SA with less than 10°. The optimum mechanical properties of the superhydrophobic coatings were achieved when the addition of C9 resin concentration was 6 wt.%. Superhydrophobic coatings that were applied to a variety of substrates, regardless of the substrate surfaces and geometry, were made using a two-step spraying technique. Additionally, SBS/C9-SiO$_2$ coatings exhibit outstanding mechanical properties, excellent self-cleaning properties, and corrosion resistance. Moreover, there are numerous application possibilities for SBS/C9-SiO$_2$ coatings, which can be prepared in a straightforward, inexpensive manner and utilized for corrosion resistance, oil and water separation, and other purposes.

Author Contributions: Conceptualization, B.X.; methodology, B.X., Y.Z. and S.G.; formal analysis, B.X. and Y.Z.; investigation, Y.Z. and S.G.; resources, Q.X. and M.H.; data curation, Y.Z.; writing—original draft preparation, Y.Z.; writing—review and editing, B.X., Y.Z., C.L. and Z.N.; visualization, B.X. and Y.Z.; supervision, B.X., Q.X., M.H., C.L. and Z.N.; project administration, B.X. and Y.Z. All authors have read and agreed to the published version of the manuscript.

Institutional Review Board Statement: Not applicable.

Informed Consent Statement: Not applicable.

Data Availability Statement: Not applicable.

Conflicts of Interest: The authors declare no conflict of interest.

References

1. Yang, J.; Long, F.; Wang, R.; Zhang, X.; Yang, Y.; Hu, W.; Liu, L. Design of mechanical robust superhydrophobic Cu coatings with excellent corrosion resistance and self-cleaning performance inspired by lotus leaf. *Colloids Surf. A* **2021**, *627*, 127154. [CrossRef]
2. Bai, F.; Wu, J.T.; Gong, G.M.; Guo, L. Biomimetic "Water Strider Leg" with Highly Refined Nanogroove Structure and Remarkable Water-Repellent Performance. *ACS Appl. Mater. Inter.* **2014**, *6*, 16237–16242. [CrossRef] [PubMed]
3. Wang, Z.; Li, Z.; Feng, X.M.; Jiao, X.M.; Zhang, X.M.; Niu, S.C.; Han, S.C.; Ben, L.Q. Rapid Fabrication of Bio-inspired Antireflection Film Replicating from Cicada Wings. *J. Bionic. Eng.* **2020**, *17*, 34–44. [CrossRef]
4. Zhang, H.L.; Ji, X.X.; Liu, X.X.; Ren, J.P.; Tao, F.R.; Qiao, C.D. Versatile, mechanochemically robust, sprayed superomniphobic coatings enabling low surface tension and high viscous organic liquid bouncing. *Chem. Eng. J.* **2020**, *402*, 126160. [CrossRef]
5. Yi, K.; Fu, S.Y.; Huang, Y.B. Nanocellulose-based superhydrophobic coatings with acid resistance and fluorescence. *Prog. Org. Coat.* **2022**, *168*, 106911. [CrossRef]
6. Bao, Y.; Chang, J.X.; Zhang, Y.X.; Chen, L. Robust superhydrophobic coatings with hollow SiO_2/PAA-b-PS Janus microspheres for self-cleaning and oil-water separation. *Chem. Eng. J.* **2022**, *446*, 136959. [CrossRef]
7. Wang, X.K.; Zeng, J.; Yu, X.Q.; Zhang, Y.F. Superamphiphobic coatings with polymer-wrapped particles: Enhancing water harvesting. *J. Mater. Chem. A* **2019**, *7*, 5426–5433. [CrossRef]
8. Chen, T.C.; Guo, J.; Zhang, Y.Y.; Hu, N.N.; Zhang, J.L. Superamphiphobic triple-scale micro-/nanostructured aluminum surfaces with self-cleaning and anti-icing properties. *J. Mater. Sci.* **2021**, *56*, 15463–15480. [CrossRef]
9. Zhang, B.B.; Xu, W.C. Superhydrophobic, superamphiphobic and SLIPS materials as anti-corrosion and anti-biofouling barriers. *New J. Chem.* **2021**, *45*, 15170–15179. [CrossRef]
10. Guo, C.L.; Ding, H.; Xie, M.X.; Zhang, H.Q.; Hong, X.Y.; Sun, L.Y.; Ding, F.C. Multifunctional superamphiphobic fluorinated silica with a core-shell structure for anti-fouling and anti-corrosion applications. *Colloids Surf. A* **2021**, *615*, 126155. [CrossRef]
11. Liu, Y.; Gu, H.; Jia, Y.; Liu, J.; Zhang, H.; Wang, R.; Zhang, B.; Zhang, H.; Zhang, Q. Design and preparation of biomimetic polydimethylsiloxane (PDMS) films with superhydrophobic, self-healing and drag reduction properties via replication of shark skin and SI-ATRP. *Chem. Eng. J.* **2019**, *356*, 318–328. [CrossRef]
12. Xu, S.S.; Wang, Q.; Wang, N. Fabrication of pre-wetting induced superamphiphobic meshes for on-demand oil-water separation of light or heavy oil-water mixtures. *Colloids Surf. A* **2020**, *602*, 125095. [CrossRef]
13. Chen, J.H.; Liu, Z.H.; Wen, X.F.; Xu, S.P.; Wang, F.; Pi, P.H. Two-Step Approach for Fabrication of Durable Superamphiphobic Fabrics for Self-Cleaning, Antifouling, and On-Demand Oil/Water Separation. *Ind. Eng. Chem. Res.* **2019**, *58*, 5490–5500. [CrossRef]
14. Mahadik, S.A.; Mahadik, S.S. Surface morphological and topographical analysis of multifunctional superhydrophobic sol-gel coatings. *Ceram. Int.* **2021**, *47*, 29475–29482. [CrossRef]
15. Su, D.; Huang, C.Y.; Hu, Y.; Jiang, Q.W.; Zhang, L.; Zhu, Y.F. Preparation of superhydrophobic surface with a novel sol-gel system. *Appl. Surf. Sci.* **2011**, *258*, 928–934. [CrossRef]
16. Fang, Z.P.; Luo, W.; Hu, H.L.; Xia, M.; Sun, Z.G.; Zhang, Y.H.; He, P.X. Ice-template triggered roughness: A facile method to prepare robust superhydrophobic surface with versatile performance. *Prog. Org. Coat.* **2019**, *135*, 345–351. [CrossRef]
17. Wang, J.P.; Wu, Y.L.; Zhang, D.G.; Li, L.H.; Wang, T.; Duan, S.Y. Preparation of superhydrophobic flexible tubes with water and blood repellency based on template method. *Colloids Surf. A* **2020**, *587*, 124331. [CrossRef]
18. Cho, S.W.; Kim, J.H.; Lee, H.M.; Chae, H.; Kim, C.K. Superhydrophobic Si surfaces having microscale rod structures prepared in a plasma etching system. *Surf. Coat. Tech.* **2016**, *306*, 82–86. [CrossRef]
19. Dimitrakellis, P.; Travlos, A.; Psycharis, V.P.; Gogolides, E. Superhydrophobic Paper by Facile and Fast Atmospheric Pressure Plasma Etching. *Plasma. Process. Polym.* **2017**, *14*, 1600069. [CrossRef]
20. Nguyen-Trig, P.; Altiparmak, F.; Nguyen, N.; Tuduri, L.; Ouellet-Plamondon, C.M.; Prud'homme, R.E. Robust Superhydrophobic Cotton Fibers Prepared by Simple Dip-Coatings Approach Using Chemical and Plasma-Etching Pretreatments. *ACS Omega* **2019**, *4*, 7829–7837. [CrossRef]
21. Bayram, F.; Mercan, E.S.; Karaman, M. One-step fabrication of superhydrophobic-superoleophilic membrane by initiated chemical vapor deposition method for oil-water separation. *Colloid. Polym. Sci.* **2021**, *299*, 1469–1477. [CrossRef]
22. Tombesi, A.; Li, S.H.; Sathasivam, S.; Page, K.; Heale, F.L.; Pettinari, C.; Carmalt, C.J.; Parkin, I.P. Aerosol-assisted chemical vapour deposition of transparent superhydrophobic film by using mixed functional alkoxysilanes. *Sci. Rep.* **2019**, *9*, 7549. [CrossRef] [PubMed]
23. Wang, H.J.; Zhang, Z.H.; Wang, Z.K.; Liang, Y.H.; Cui, Z.Q.; Zhao, J.; Li, X.J.; Ren, L.Q. Multistimuli-Responsive Microstructured Superamphiphobic Surfaces with Large-Range, Reversible Switchable Wettability for Oil. *ACS Appl. Mater. Inter.* **2019**, *11*, 28478–28486. [CrossRef] [PubMed]
24. Rasitha, T.P.; Philip, J. Optimal condition for fabricating mechanically durable superhydrophobic titanium surface by rapid breakdown anodization: Self cleaning and bouncing characteristics. *Appl. Surf. Sci.* **2022**, *585*, 152628.
25. Rasitha, T.P.; Krishna, D.N.G.; Thinaharan, C.; Vanithakumari, S.C.; Philip, J. Optimization of coating parameters for fabrication of robust superhydrophobic (SHP) aluminum and evaluation of corrosion performance in aggressive medium. *Prog. Org. Coat.* **2022**, *172*, 107076. [CrossRef]
26. Wang, T.; Lv, C.; Ji, L.L.; He, X.; Wang, S. Designing Re-Entrant Geometry: Construction of a Superamphiphobic Surface with Large-Sized Particles. *ACS Appl. Mater. Inter.* **2020**, *12*, 49155–49164. [CrossRef]

27. Han, X.T.; Peng, J.Y.; Jiang, S.H.; Xiong, J.; Song, Y.; Gong, X. Robust Superamphiphobic Coatings Based on Raspberry-like Hollow SnO$_2$ Composites. *Langmuir* **2020**, *36*, 11044–11053. [CrossRef]

28. Chatzigrigoriou, A.; Karapanagiotis, I.; Poulios, I. Superhydrophobic coatings based on siloxane resin and calcium hydroxide nanoparticles for marble protection. *Coatings* **2020**, *10*, 334. [CrossRef]

29. Meng, J.Q.; Lin, S.S.; Xiong, X.P. Preparation of breathable and superhydrophobic coatings film via spray coatings in combination with vapor-induced phase separation. *Prog. Org. Coat.* **2017**, *107*, 29–36. [CrossRef]

30. Xiong, X.; Xie, F.; Meng, J. Preparation of superhydrophobic porous coatings film with the matrix covered with polydimethyl-siloxane for oil/water separation. *Prog. Org. Coat.* **2018**, *125*, 365–371. [CrossRef]

31. Xi, Y.; Yang, Z.; Zhang, J. Fabrication of superhydrophobic bilayer composite coatings for roof cooling and cleaning. *Constr. Build. Mater.* **2021**, *291*, 123283. [CrossRef]

32. Huang, Y.; Chen, B.; Lv, Z.; Guo, F.; Huang, C. A cost-effective method for robust and anti-corrosive superhydrophobic coatings. *SN Appl. Sci.* **2019**, *1*, 612. [CrossRef]

33. Karapanagiotis, I.; Manoudis, P.N. Superhydrophobic and superamphiphobic materials for the conservation of natural stone: An overview. *Constr. Build. Mater.* **2022**, *320*, 126175. [CrossRef]

34. Jiao, X.; Li, M.; Yu, X.; Wong, W.S.Y.; Zhang, Y. Oil-immersion stable superamphiphobic coatings for long-term super liquid-repellency. *Chem. Eng. J.* **2021**, *420*, 127606. [CrossRef]

35. Wei, J.; Li, B.; Jing, L.; Tian, N.; Zhao, X.; Zhang, J. Efficient protection of Mg alloy enabled by combination of a conventional anti-corrosion coatings and a superamphiphobic coatings. *Chem. Eng. J.* **2020**, *390*, 124562. [CrossRef]

36. Nie, X.; Hou, T.; Yao, H.; Li, Z.; Zhou, X.; Li, C. Effect of C9 petroleum resins on improvement in compatibility and properties of SBS-modified asphalt. *Pet. Sci. Technol.* **2019**, *37*, 1704–1712. [CrossRef]

37. Mallegol, J.; Bennett, G.; McDonald, P.J.; Keddie, J.L.; Dupont, O. Skin development during the film formation of waterborne acrylic pressure-sensitive adhesives containing tackifying resin. *J. Adhes.* **2006**, *82*, 217–238. [CrossRef]

38. Karademir, A.; Aydemir, C.; Yenidogan, S.; Kandirmaz, E.A.; Kiter, R.G. The use of natural (*Pinus pinaster*) resin in the production of printing ink and the printability effect. *Color. Res. Appl.* **2020**, *45*, 1170–1178. [CrossRef]

39. Schaur, A.; Unterberger, S.; Lackner, R. Impact of molecular structure of SBS on thermomechanical properties of polymer modified bitumen. *Eur. Polym. J.* **2017**, *96*, 256–265. [CrossRef]

40. Zhang, W.; Qiu, L.; Liu, J.; Hu, K.; Zou, L.; Chen, Y.; Yang, C.; Wang, F.; Zang, J. Modification mechanism of C9 petroleum resin and its influence on SBS modified asphalt. *Constr. Build. Mater.* **2021**, *306*, 124740. [CrossRef]

41. Wu, H.; Chen, P.; Chen, C.; Zhang, W.; Sun, X. Effect of Aromatic Petroleum Resin on Microstructure of SBS Modified Asphalt. *Adv. Mater. Sci. Eng.* **2022**, *2022*, 5136748. [CrossRef]

42. Ryu, D.Y.; Kim, J.K. The aromatic hydrocarbon resins with various hydrogenation degrees Part 2. The adhesion and viscoelastic properties of the mixtures of resins and block copolymers. *Polymer* **2000**, *41*, 5207–5218. [CrossRef]

43. Koch, K.; Bhushan, B.; Barthlott, W. Multifunctional surface structures of plants: An inspiration for biomimetics. *Prog. Mater. Sci.* **2009**, *54*, 137–178. [CrossRef]

44. Shao, H.; Yu, Y.; Li, Y.; Shuai, M.; He, Z.; Tang, C.; Li, X.; Mei, J.; Fu, Q. Building a mechanically stable polydimethylsiloxane/silica superhydrophobic coatings on poly(chloro-p-xylylene) film by introducing a polydimethylsiloxane adhesive layer. *Surf. Coat. Technol.* **2018**, *350*, 201–210. [CrossRef]

45. Zhou, Z.; Chen, G. Preparation, Performance, and modification mechanism of high viscosity modified asphalt. *Constr. Build. Mater.* **2021**, *310*, 125007. [CrossRef]

46. Li, H.; Xin, L.; Zhang, K.; Yin, X.L.; Yu, S.R. Fluorine-free fabrication of robust self-cleaning and anti-corrosion superhydrophobic coatings with photocatalytic function for enhanced anti-biofouling property. *Surf. Coat. Technol.* **2022**, *438*, 128406. [CrossRef]